Processes controlling lithium isotopic distribution in contact aureoles: A case study of the Florence County pegmatites, Wisconsin

Xiao-Ming Liu, Roberta L. Rudnick, and Saswata Hier-Majumder
Department of Geology, University of Maryland, College Park, Maryland 20742, USA
(xliu1235@umd.edu)

Mona-Liza C. Sirbescu
Geology Department, Central Michigan University, 314 Brooks Hall, Mt. Pleasant, Michigan 48859, USA

[1] Li isotopes may be useful tracers of fluid flow in a number of geological environments and case studies of contact aureoles have highlighted the very large Li isotopic fractionation that can be generated in these settings. However, the amount of isotopic fractionation and the distance that Li travels into the country rocks vary greatly from place to place. Seeking to identify the parameters that govern Li distribution in contact aureoles, we apply a combination of Li isotope analyses, 1-D diffusion and 2-D advection-diffusion modeling to two country rock profiles adjacent to Li-rich pegmatite dikes from the Florence County pegmatite field, Wisconsin. Although less than ~3 m thick, the pegmatite sheets have a large impact on the Li budget of the country rocks (amphibolites and schists); Li is enriched in adjacent country rocks by up to a factor of 20 over more distant amphibolites and schists. Li from the pegmatite has traveled more than 50 m into the country rocks, and Li isotopes are systematically fractionated with distance from the contacts (with δ^7Li varying from +6 at the contact to −7 at 30 m from the contact in one case). These observations are consistent with diffusive fractionation of Li through an advecting grain-boundary fluid. Both one-dimensional diffusion and two-dimensional advection-diffusion models fail to reproduce the exact Li distribution in the profiles, suggesting that fluid advection, coupled with heterogeneous permeability, plays an important role in determining the final Li distribution within the contact aureoles.

Liu, X.-M., R. L. Rudnick, S. Hier-Majumder, and M.-L. C. Sirbescu (2010), Processes controlling lithium isotopic distribution in contact aureoles: A case study of the Florence County pegmatites, Wisconsin, *Geochem. Geophys. Geosyst.*, *11*, Q08014, doi:10.1029/2010GC003063.

1. Introduction

[2] Fluid flow is important in the continental crust, at least down to depths of 10 to 15 km, where hydrous fluids may change the physical and chemical properties of the crust, such as its thermal structure and chemical composition, as they interact with rock [e.g., *Ague*, 2003; *Deming*, 1994; *Ferry*, 1994]. Contact aureoles provide a natural laboratory in which to study fluid-rock interactions due to the pressure and temperature gradients created by shallow igneous intrusion into colder country rocks. Stable isotopes are especially useful for tracing flow fluid through metamorphic country rocks [*Baumgartner and Valley*, 2001, and references therein].

[3] Oxygen isotopes, in particular, have been widely used in studying metamorphic fluid flow in contact aureole settings. Models of one-dimensional oxygen isotope transport in homogeneous porous rocks provide basic understanding of fluid-rock interactions [e.g., *Bickle and McKenzie*, 1987; *Bowman and Willett*, 1991]. However, because fluid flow direction (up-down and toward-away from pluton) [*Ferry*, 1994; *Ferry et al.*, 2002] and permeability structure of the country rocks play important roles in controlling oxygen isotope distribution [*Cui et al.*, 2001], 1-D fluid flow models are often not adequate for describing the isotope transport processes. Two-dimensional flow fluid models can incorporate fluid infiltration direction and structure of country rocks (e.g., permeability structure) during contact metamorphism. Starting from the pioneering work of *Norton and Taylor* [1979], 2-D reactive flow models for oxygen isotopes have successfully reproduced heterogeneous fluid flow patterns [e.g., *Cook et al.*, 1997; *Cui et al.*, 2002].

[4] Lithium is a trace element that preferentially partitions into aqueous fluids relative to most minerals [*Brenan et al.*, 1998a] and hence may be useful for tracing fluid flow through rock. Recently, lithium isotopes have been used to investigate fluid-rock interactions in contact aureole settings [*Marks et al.*, 2007; *Teng et al.*, 2006a, 2007]. Lithium isotopes have a few advantages in tracing fluid flow in these settings. First, as stated above, Li is fluid soluble [*Brenan et al.*, 1998b] and so becomes enriched in the fluid relative to the rock. Second, it diffuses faster than most other geochemical tracers [*Richter et al.*, 2003]. Thus, Li can trace diffusive processes on a shorter timescale and/or greater length scale compared to other isotopic tracers. Third, Li is moderately incompatible [*Brenan et al.*, 1998a], so it partitions preferentially into melts

during partial melting and becomes enriched in evolved plutons, such as Li-rich granitic pegmatites and their associated aqueous fluid/melt, which can act as the Li source for tracing fluid flow in contact aureoles. Last, there is a large mass difference (~17%) between the two stable isotopes of Li, which gives rise to significant isotopic fractionation in various geological environments, especially during diffusion [e.g., *Lundstrom et al.*, 2005; *Richter et al.*, 2003; *Teng et al.*, 2006a]. Therefore, Li can be used as a geochemical tracer for fluid-rock interactions in the continental crust.

[5] Recent observations from contact aureoles around igneous intrusions reveal large and systematic changes in δ^7Li, which is defined as

$$\delta^7Li = \left[\left(^7Li \big/ ^6Li \right)_{sample} \big/ \left(^7Li \big/ ^6Li \right)_{standard} - 1 \right] \times 1000,$$

where the standard used is L-SVEC [*Flesch et al.*, 1973]. However, the behavior of Li varies from one setting to the next.

[6] The Li-rich Tin Mountain pegmatite, South Dakota, intruded into relatively Li-poor country rocks. A profile through an adjacent amphibolite shows both Li concentration and δ^7Li decreasing dramatically with distance from the pegmatite contact [*Teng et al.*, 2006a]. A 1-D diffusion model is used to explain the geochemical observations, indicating diffusion-driven lithium isotopic fractionation through pore fluids [*Teng et al.*, 2006a]. However, the profile ends at ~ 10 m distance from the contact, at the top of a cliff face, and so the total distance over which Li moved is unknown.

[7] In contrast to the Tin Mountain pegmatite, the Onawa granodiorite, Maine, is not particularly Li enriched (45 $\mu g/g$) and intrudes metapelites that have considerably higher Li concentrations (64 to 124 $\mu g/g$) [*Teng et al.*, 2007]. Here, no obvious lithium isotopic fractionation was observed in the surrounding contact metamorphic aureole. However, the length scale of the measured section (~1.5 km) is much greater than the previous example, and only two retrogressed samples were taken within 300 m of the contact, so any existing Li isotope fractionation (within 100 m of the contact) may not have been observed.

[8] The second locality where Li isotope fractionation was observed in country rocks is the Ilímaussaq intrusion, southern Greenland. Here, an augite syenite (25 $\mu g/g$ Li) intrudes an I-type granite with lower Li concentration (~11 $\mu g/g$) [*Marks et al.*, 2007]. Despite the relatively small difference in Li con-

centrations between the intrusion and country rocks, significant Li isotopic fractionation was observed in both the intrusion and the country rock with distance from the contact. A 1-D diffusion model is used to explain the Li isotopic distribution in the granitic country rock, through which Li traveled between 5 and 40 m [*Marks et al.*, 2007]. The exact distance that Li diffused into the country rocks is not well constrained due to a gap in the sampling.

[9] Both the Tin Mountain and the Ilímaussaq case studies adopted semi-infinite 1-D diffusion models, which have some limitations. First, multiple pegmatite intrusions (as seen in one of the profiles investigated here) cannot be modeled. In addition, both case studies estimated very large minimum Li diffusion coefficients, on the order of 10^{-8} m²/s. Such rapid inferred diffusion may indicate that processes in addition to grain boundary diffusion, such as fluid advection, may have influenced the Li distribution in the country rocks.

[10] The variability of Li distribution among the three previously studied contact aureoles raises the question: what are the most important mechanisms controlling Li isotope distribution in contact aureole settings? Two end-member mechanisms may control Li transport in a contact aureole: (1) a diffusion-only mechanism, in which Li travels outwards through a stagnant grain-boundary fluid due to a gradient in chemical potential between the intrusion and the Li-poor country rocks; and (2) an advection-diffusion mechanism in which a Li-rich magmatic fluid released from the intrusion follows flow patterns controlled by intrusion pressure, fluid buoyancy, and permeability structure of country rocks.

[11] In this study we seek to determine the most significant mechanisms that influence lithium distribution in contact aureoles and further develop Li isotopes as a tracer of fluid flow processes in the crust. Toward this end, lithium concentration and isotopic composition of two different Li-rich pegmatite intrusions and their country rocks were measured in the Florence County pegmatite field, Wisconsin. Interpretation of the results was aided by 1-D diffusion and 2-D fluid flow numerical models, which allow identification of the most important parameters influencing Li distribution in these settings and provide constraints on possible mechanisms for mass transport.

2. Geological Settings and Samples

[12] Samples in this study are from the Florence County pegmatite field in northeastern Wisconsin,

~15 km south of the border with northern Michigan (Figure S1 in Text S1 in the auxiliary material).[1] Here, post-tectonic granitic pegmatite dikes intrude rocks of the Penokean Orogen, a 1400 km long fold-and-thrust belt that formed during accretion and collision of the early Proterozoic Wisconsin Magmatic Terrane onto the southern margin of the Archean Superior Province. The pegmatite field is located about 5 km south of the Niagara Fault Zone [*Sirbescu et al.*, 2008, and references therein].

[13] The Florence county pegmatite dikes are believed to be associated with ~1760 Ma post-tectonic peraluminous granites that were intruded at depths of 10–11 km [*Holm et al.*, 2005]. The closest known exposures (Bush Lake granite) occur at around 3–4 km SW of our study area. The country rocks surrounding the pegmatites belong to the 1866 ± 39 Ma Quinnesec Formation [*Sims et al.*, 1992], an early Penokean unit composed of mafic to felsic metavolcanic rocks. These rocks are regionally metamorphosed to amphibolites and felsic metatuffs, at greenschist and amphibolite facies. Minor metasedimentary layers, such as quartz-mica schists, iron formation, and quartzites are also present [*Sirbescu et al.*, 2008].

[14] Samples were collected adjacent to two highly differentiated, spodumene-bearing pegmatites (Figure 1), namely, along the Hwy 101 road cut that exposes the northern segment of the King's-X pegmatite (first recognized by *Richardson et al.* [1995] and *Falster et al.* [2005], hereafter referred to as the KX profile) and in outcrops adjacent to the highstanding Animikie Red Ace pegmatite (ARA profile [*Falster et al.*, 1996]). The pegmatites are interpreted to have intruded as water-rich magmas that cooled rapidly [*Sirbescu et al.*, 2009]. In addition, regional samples were collected far away from any known pegmatites (e.g., a few hundred meters to several thousand meters away from the pegmatites, Figure S2 in Text S1). Thus, the regional samples are regarded as unaffected by pegmatite intrusions. Petrographic descriptions of pegmatites, country rocks and regional samples are provided in Table S1 in Text S1. More petrographic and mineralogical details are given by *Falster et al.* [1996], *Richardson* [1998], and *Sirbescu et al.* [2009].

2.1. King's-X Profile

[15] The ~3 m wide King's-X pegmatite is exposed at the western end of a road cut that extends for

---
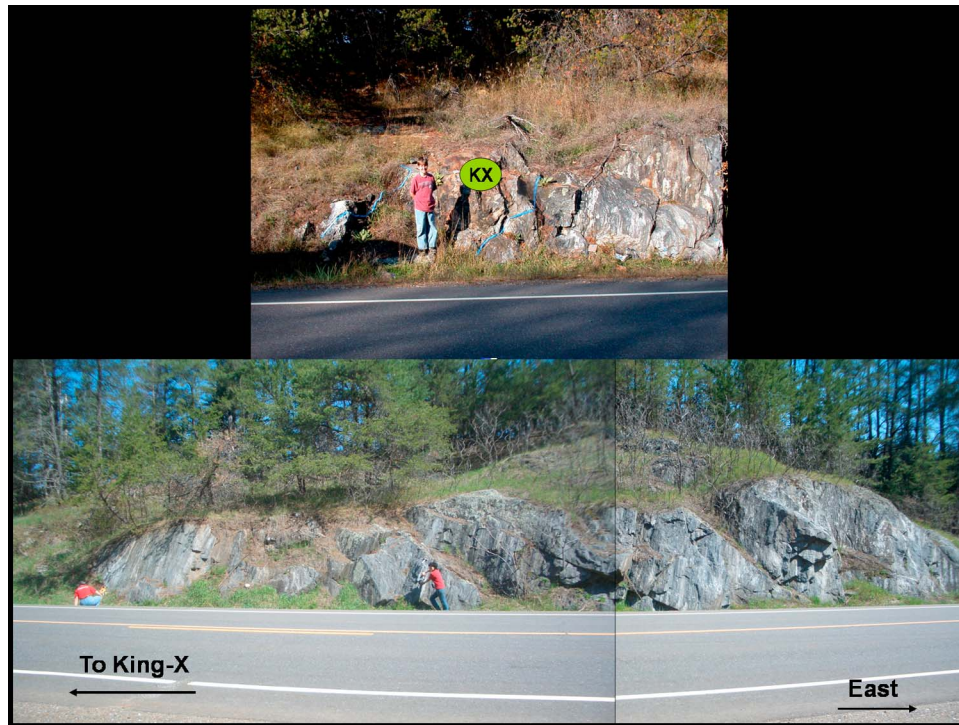
Figure 1. Field photos of the King's-X profile. The KX road cut is along Hwy 101. (top) The KX pegmatite, located in the west side of the profile, with a 1.4 m person for scale; the blue tape marks the pegmatite-country rock boundaries. (bottom) The east side of the KX profile. The whitish subvertical streaks mark the carbonate layers within amphibolite.

~70 m (Figure 1). The pegmatite intrudes discordantly into steeply dipping Quinnesec formation rocks. On the whole, the country rocks of the KX profile show banded lithological variations sub-parallel to the road cut, including biotite-chlorite schists, carbonate-bearing amphibolite, and quartzite layers that are cm to dm thick.

[16] The spodumene and amblygonite-bearing King's-X pegmatite occurs at the western end of the road cut (Figure 1). From our field and thin-section observations, this portion of the pegmatite is composed of dark gray feldspar and quartz, muscovite, dark blue to black tourmaline and spodumene. Common accessory minerals include amblygonite-montebrassite and other Li phosphates.

[17] The KX country rocks mainly consist of alternating layers of dark amphibolite/biotite schists with white carbonate and quartzite layers. Amphibolites are mainly composed of amphibole, plagioclase, quartz and carbonate; some amphibolites contain biotite, chlorite, opaques, and titanite. Chlorite mostly occurs on the rims of amphibole. Biotite schists are composed of biotite, quartz, feldspar, and carbonate with or without chlorite, tourmaline, epidote,

opaques, and titanite. Quartzites contain quartz, amphibole and opaques with or without biotite, carbonate, chlorite, and titanite. In all samples, chlorite, which is a common accessory mineral in the KX country rocks, appears to be an alteration product of amphibole or biotite. In addition, coarse biotite, black tourmaline, and minor fluorite are found along thin veinlets or metasomatic replacements in the immediate vicinity of the pegmatite (within 0.5 m from the contact).

[18] A 0.1 m wide, nearly vertical vein intruded into the country rocks approximately 16.5 m from the KX pegmatite contact consists of feldspar, quartz and minor black tourmaline. This quartzo-feldspathic vein is undeformed, but unlike the KX pegmatite, does not have a visible metasomatic influence on the mineralogy of the country rocks. The relative timing of intrusion between the KX pegmatite and this vein is unknown.

[19] Twenty-nine country rock samples were collected along a ~40 m wide traverse along the KX road cut, including both sides of the KX dike. In addition, the KX pegmatite dike, and the quartzo-feldspathic vein were sampled.
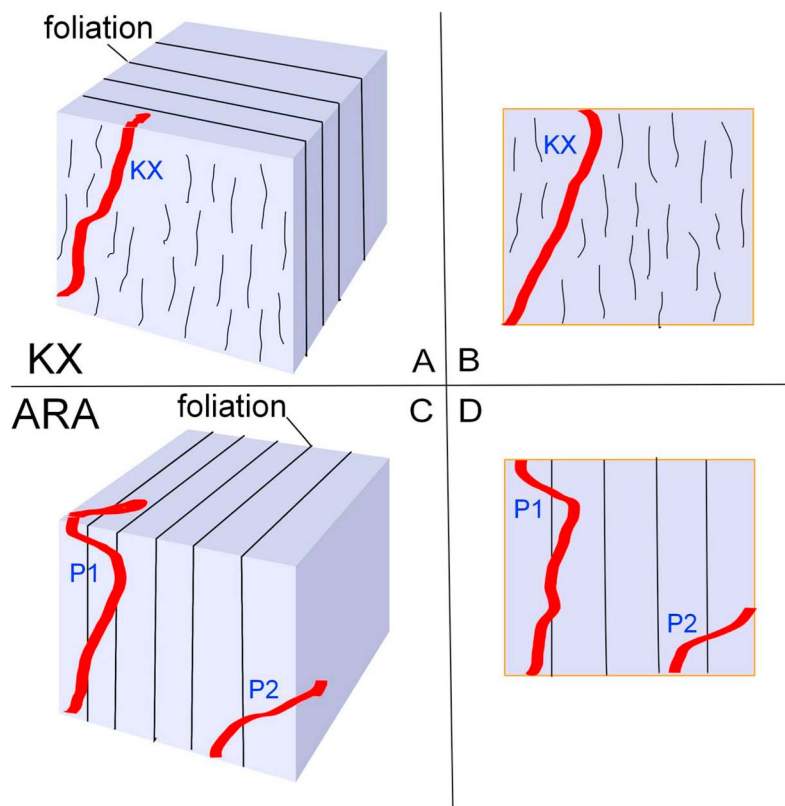
Figure 2. Schematic field geometry of the pegmatites and their country rocks. Pegmatite dikes are represented in red and the country rocks are represented in blue. Solid and dashed black lines represent foliations and lithological layers, respectively. (a and b) The 3-D and 2-D simplified geometry of King's-X road cut profile, respectively. (c and d) The 3-D and 2-D model simplified geometry of Animikie Red Ace profile, respectively.

2.2. Animikie Red Ace Profile

[20] The Animikie Red Ace (ARA) profile is composed of two pegmatite dikes separated by ~60 m of country rocks. The larger pegmatite, P1, is up to 2.5 m wide and the smaller one, P2, is ~0.6 m wide. The P1 pegmatite is a mineralogically zoned, spodumene-lepidolite bearing dike, described previously as the ARA southern segment [*Falster et al.*, 1996]. The P1 magma is interpreted to have intruded at around 700°C and cooled to <400°C rapidly (within 50 days) [*Sirbescu et al.*, 2008]. The P2 pegmatite appears to have fewer mineral phases, and consists of feldspar, quartz and micas. The relative timing of intrusion of these two dikes is not known. The country rocks consist of schist within the first 45 m from the contact with P1, and amphibolite for the remainder of the profile to P2.

[21] Two bulk samples were collected from the P1 pegmatite and one was collected from the P2 pegmatite. One P1 sample, ARA1a, is massive and contains feldspar, quartz, lepidolite, and minor pink and blue tourmaline. The other P1 sample, ARA1b, is composed of pink tourmaline, quartz, feldspar and micas. The P2 pegmatite sample, 08-P-06, consists of feldspar, quartz, and micas with rare blue apatite and black tourmaline.

[22] The ARA country rocks display vertical foliation that is roughly perpendicular to the exposure surface (Figure 2). P1 and P2 are subconcordant to the foliation. Biotite schists are mainly composed of quartz, biotite, and feldspar with or without amphibole, carbonate, chlorite, epidote, muscovite and opaques. Amphibole and epidote are unusual minerals for a metapelite, suggesting that these rocks may be metavolcanic in origin. Amphibolites are mainly composed of amphibole, feldspar and quartz, with or without biotite, epidote, garnet and opaques. Epidote and chlorite are likely secondary minerals, especially in the case of chlorite, which is mostly present on the rims of the amphibole. Fifteen country rock

samples were collected within a ~60 m wide traverse between the two pegmatites.

2.3. Regional Samples

[23] Regional samples, five schists and two amphibolites, were collected from outcrops that are hundreds of meters to several kilometers away from the pegmatites (Figure S2 in Text S1). In thin-section, both schists and amphibolites have similar mineralogy to their counterparts from the KX and ARA profiles, except that regional amphibolites lack the intercalated carbonate layers found in the KX profile. Schists are mainly composed of quartz, biotite, and feldspar, with or without amphibole, carbonate, chlorite, epidote, and opaques. Amphibolites are mainly composed of amphibole, feldspar and quartz, with or without biotite, chlorite and opaques. Unlike the profile samples, the regional samples show no obvious evidence of alteration and they lack tourmaline; chlorite appears to be a primary mineral because it occurs in the groundmass and does not rim amphibole. Primary chlorite is consistent with the peak metamorphic conditions of the country rocks, which are at greenschist to amphibolite facies.

3. Analytical Methods

3.1. Lithium Analyses of Whole Rocks

[24] Detailed procedures for sample dissolution and column chemistry are described by *Rudnick et al.* [2004] and instrumental analysis is described by *Teng et al.* [2004]. A brief description of these methods is provided below.

[25] Rock samples were cut and then ground to powders using a corundum jaw crusher after the weathered surfaces of samples were sawn off. Rock powders were dissolved using a roughly 3:1 mixture of HF and HNO_3 in Savillex® screw-top beakers on a hot plate (T ≈ 90°C), followed by HNO_3 and HCl addition until all powder was dissolved and the solution was clear.

[26] Solutions were purified using cation exchange columns (BioRad AG50W-x12). Four chromatographic columns were used, modified from the procedure described by *Moriguti and Nakamura* [1998]. The first two columns eliminate major element cations in sample solutions with 2.5M HCl and 0.15M HCl, respectively. The third column separates Na from Li with 30% ethanol in 0.5M HCl and the fourth column is a repeat of the third. Yields are

determined to be greater than 95% [*Marks et al.*, 2007].

[27] Whole rock solutions were analyzed using the Nu Plasma Multi Collector-Inductively Coupled Plasma-Mass Spectrometer (MC-ICP-MS) at the University of Maryland. Standard bracketing, using L-SVEC, was performed for all analyses. The Li isotopic composition is reported as δ^7Li. The external precision, based on 2σ of duplicate runs of pure Li standard solutions, is ≤±1.0‰. For example, IRMM-016 run during the course of these analyses (June 2008 to June 2009) gives $\delta^7Li = -0.5 \pm 0.9‰$ (2σ, n = 25); and the in-house standard, UMD-1, gives $\delta^7Li = 54.4 \pm 1.0‰$ (2σ, n = 22) (see Table S2 in Text S1). In addition, several USGS reference rocks were run repeatedly (Table S3 in Text S1). BHVO-1 yielded δ^7Li of 4.0 ± 1.2 (n = 4) cf. 4.3 to 5.8 in the literature [see *Rosner et al.*, 2007, and references therein], AGV-1 yielded δ^7Li of 4.6 ± 0.7 (n = 6), compared to 6.7 for AGV-1 from *Magna et al.* [2004], and G-2 yielded δ^7Li of 0.3 ± 1.9 (n = 4), compared to −1.2 from *James and Palmer* [2000] and −0.3 from *Pistiner and Henderson* [2003].

3.2. Amphibole Compositions

[28] Major element compositions of amphiboles from the KX profile were determined using the Electron Probe Microanalyzer (EPMA) at the University of Maryland. An accelerating voltage of 15 kV and a cup current of 20 nA were used for all the analyses. Raw X-ray counts were corrected using the ZAF algorithm. Calibration was performed using natural mineral standards. The CaO content in amphiboles shows little variation (multiple measurements of the same sample show 2σ variation of <0.9%). Major element data are reported in Table S4 in Text S1.

[29] The Li concentrations of amphiboles from amphibolites were determined using laser ablation ICP-MS of thin sections and mounts (Element II single collector-ICP-MS coupled with a 213 nm wavelength laser at the University of Maryland). Multiple spots on multiple amphibole grains within a sample were analyzed with a spot size of 30–40 μm and ablation energy of 2–3 J/cm². NIST610 (CaO = 11.4 wt. %), run at the beginning and the end of each sample set of ≤16 analyses, was used as the external standard and ^{43}Ca was used as the internal standard to correct for differences in ablation yield. Data were processed using a modified version of the LAMTRACE software. Li concentrations of BCR-2g (Table S5 in Text S1) are

Table 1.   Li Concentration and Isotopic Composition of Whole Rock Samples in the KX and ARA Pegmatites and Country Rocks[a]

Sample[b]	Rock Type	[Li] (μg/g)	δ^7Li (‰)	Distance (m)
King's X, Latitude 45.85208°N, Longitude 88.35409°W				
KX05	Schist	592	−7.8	−8.5
KX04 (2)	Schist	426	−7.9	−6.5
KX03 (2)	Schist	494	1.6	−3.2
KX02 (2)	Schist	919	−0.8	−3.05
KX01	Pegmatite	31	10.2	−1.45
407-Db[c]	Spodumene	22330	1.5	−1.45
LP32	Schist	2618	5.0	0
LP33b (2)	Schist	1173	1.7	0
LP31	Schist	1307	4.2	0.5
LP30 (2)	Amphibolite	56	−0.4	1.1
LP29 (2)	Amphibolite	133	−1.1	2.5
LP28	Amphibolite	220	−0.2	3.3
LP27 (2)	Quartzite	26	1.3	5.85
LP26 (2)	Quartzite	58	0.2	9.25
LP25	Quartzite	53	1.7	10.8
LP25[d]	Quartzite	54	2.2	10.8
LP24	Amphibolite	706	−3.0	12.05
LP23	Amphibolite	232	−5.1	15.1
LP22	Amphibolite	136	−4.7	15.53
LP21	Amphibolite	158	−5.2	16.25
LP1 (3)	Qtz-feld. vein	170	−0.5	16.47
LP2 (2)	Amphibolite	238	−3.0	16.5
LP2[e]	Amphibolite	236	−4.3	16.5
LP3 (2)	Amphibolite	69	−3.8	16.6
LP4 (2)	Amphibolite	167	−4.0	16.7
LP4a (2)	Amphibolite	93	−2.9	17.17
LP4b (2)	Amphibolite	146	−3.9	17.65
LP5 (2)	Amphibolite	112	−3.2	18.25
LP6 (4)	Amphibolite	146	−2.3	19.25
LP10	Amphibolite	84	−2.3	21.3
LP9	Amphibolite	130	−3.4	23.5
LP8	Amphibolite	108	−5.6	26.3
LP7 (2)	Amphibolite	102	−6.2	27.15
LP11	Amphibolite	149	−6.6	31.3
Animikie Red Ace, Latitude 45.85013°N, Longitude 88.35120°W				
ARA1a (3)	Pegmatite 1	153	5.6	0
ARA1b (2)	Pegmatite 1	666	7.7	0
ARA2a (2)	Schist	484	4.2	0.1
ARA2b (2)	Schist	160	4.0	0.45
ARA2c (2)	Schist	297	4.7	1
ARA2d (3)	Schist	160	5.0	1.16
ARA2f (2)	Schist	197	5.3	1.55
ARA2e (3)	Schist	295	5.1	1.8
ARA2g (2)	Schist	243	6.2	2.7
ARA2h (2)	Schist	139	3.4	5.8
ARA2i (2)	Schist	287	1.1	10.9
ARA2j (2)	Schist	213	2.5	14
ARA2k (2)	Schist	106	−0.6	30
ARA2l	Amphibolite	148	−3.0	45.9
ARA2n	Amphibolite	116	−2.4	46.5
ARA2o	Amphibolite	89	−0.7	50.6
ARA2p	Amphibolite	180	−1.2	57.3
08-P-06	Pegmatite 2	167	7.0	60

[a]Lithium concentration is denoted as [Li] in this and Tables 2–4. External analytical uncertainties of [Li] and δ^7Li are $\leq \pm 10\%$ (2σ) and $\leq \pm 1$ (2σ), respectively. Distance is the distance measured in meters away from the contact of a chosen pegmatite. In the KX profile, it is the distance from the KX east contact; in the ARA profile, it is the distance from the west contact of the ARA pegmatite (P1).

[b]Values in parentheses are number of re-runs on ICP-MS from the same sample solution; values reported are therefore averages of all runs.

[c]Mineral separate from the KX pegmatite.

[d]Re-dissolved and run through column chemistry from the same sample powder.

[e]Repeat column chemistry from same sample solution.

Table 2. Li Concentration and Isotopic Composition of Whole Rock Regional Amphibolites and Schists

Sample	Rock Type	[Li] (μg/g)	δ^7Li (‰)	Latitude	Longitude
QMA1	Amphibolite	19	2.8	45.8256°N	88.3404°W
QMA2	Amphibolite	13	7.0	45.8256°N	88.2881°W
QMA2[a]	Amphibolite	17	6.3	45.8256°N	88.2881°W
QFM1	Schist	17	0.7	45.8516°N	88.3404°W
QFM3	Schist	23	1.3	45.8256°N	88.2881°W
QFM4	Schist	31	1.5	45.8256°N	88.2881°W
QFM5	Schist	51	−6.1	45.7763°N	88.0566°W
QFM5[a]	Schist	36	−6.1	45.7763°N	88.0566°W
QFM6	Schist	40	1.1	45.7763°N	88.0566°W

[a]Repeat column chemistry from same sample solution.

within 9% of the nominal value and Li concentration uncertainties for the NIST610 standard vary from 0.1% to 2.8% (2σ).

4. Geochemical Results

[30] Lithium concentration and isotopic composition of the two profiles adjacent to the KX and ARA pegmatites, as well as data for regional amphibolites/schists are reported in Tables 1 and 2. Li concentration of amphiboles in selected KX amphibolite country rocks and regional amphibolites are reported in Table 3 and plotted in Figure 3. Additional analyses of Li in minerals from the pegmatites (spodumene, tourmaline and Li-rich micas) as well as fluid inclusions extracted from the pegmatites are given by X.-M. Liu (University of Maryland, Advection-diffusion controlled Li isotopic fractionation in contact aureoles: A case study from Florence County pegmatites, Wisconsin, 2009, available at http://www.lib.umd.edu/drum/handle/1903/9856) and are in Table S6 in Text S1. The whole rock δ^7Li distribution of the KX profile is also plotted

Table 3. Li Concentration of Amphiboles in Amphibolite Country Rocks of the KX Profile[a]

| Sample[b]	Mineral Phase	[Li] (μg/g)	2σ (μg/g)	Distance (m)
LP2 (5)	Amphibole	226	54	16.5
LP6 (5)	Amphibole	142	40	19.25
LP8 (4)	Amphibole	144	26	26.3
LP21 (4)	Amphibole	234	68	16.25
LP26 (4)	Amphibole	268	106	9.25
LP30 (5)	Amphibole	363	66	1.1
LP10 (7)	Amphibole	147	32	21.3
LP11 (7)	Amphibole	79	28	31.3
LP29 (7)	Amphibole	282	64	12.05
QMA1 (12)	Amphibole	32	15	~1000

[a]Uncertainties are two standard deviations of multiple measurements on multiple grains of each sample. Distance is the distance measured in meters away from the right contact of the KX pegmatite.
[b]Values in parentheses are number of measurements.

in Figure 3. Whole rock lithium concentration and isotopic composition of the Animikie Red Ace profile are plotted as a function of distance from the P1 contact in Figure 4.

4.1. King's-X Profile

[31] Li concentration of the only whole rock pegmatite sample is 31 μg/g. This is unlikely to represent the Li content of the whole pegmatite because
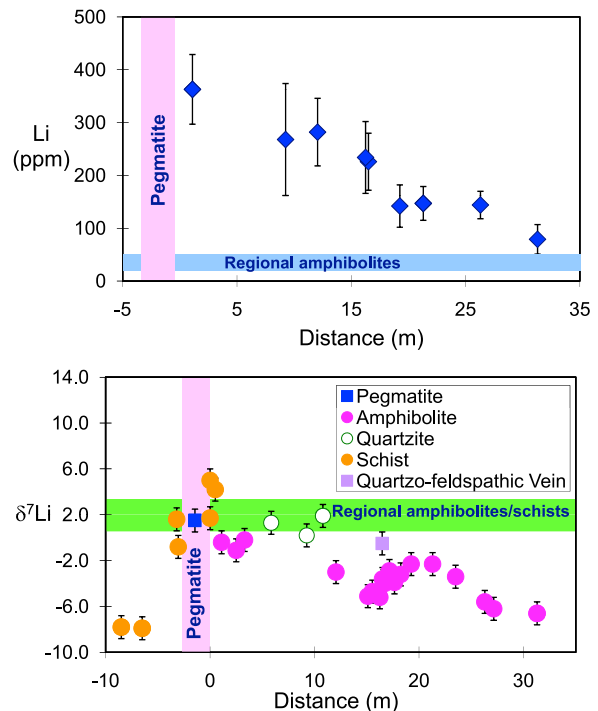
Figure 3. Plots of (top) Li concentration of amphiboles from amphibolite and (bottom) whole rock δ^7Li versus distance for the KX profile. Error bars represent two standard deviations (2σ). Horizontal blue band represents Li concentration range in amphiboles from regional amphibolites. Vertical pink band represents the KX pegmatite dike; horizontal green band indicates the δ^7Li range of regional schists and amphibolites, excluding two outliers. Data are from Tables 1 and 3.
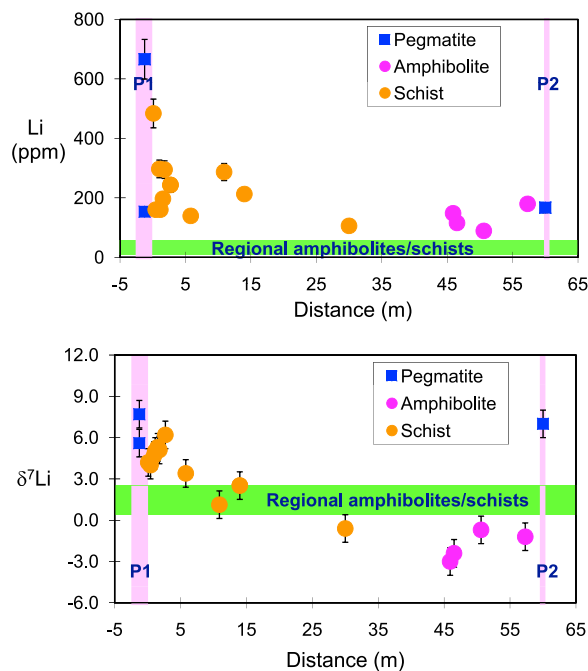
Figure 4. (top) Bulk Li concentration and (bottom) δ^7Li versus distance for the Animikie Red Ace profile. Vertical pink bands represent the P1 and P2 pegmatite dikes; horizontal green band indicates the Li concentration and δ^7Li ranges of regional schists and amphibolites in Figures 4 (top) and 4 (bottom), respectively.

the pegmatite contains spodumene and is very coarse-grained, making it difficult to obtain a representative sample. The analyzed sample is composed of quartz and feldspar, which have little Li compared to spodumene, the main Li carrier in the KX pegmatite.

[32] Li whole rock concentrations in the KX country rocks vary widely (26 to 2600 μg/g) and non-systematically with distance away from the contact (Table 1). This is likely due to the heterogeneous nature of the amphibolite and schist, which contain alternating layers of amphibole/biotite and carbonate. Li content in a whole rock sample thus depends on the proportion between the main Li-bearing phases, amphibole and biotite, and the Li-poor carbonate. Nevertheless, all country rocks, except for one quartzite, have Li concentrations greater than 50 μg/g. By contrast, lithium concentrations of the regional amphibolites and schists are much lower (Table 2), roughly 20 μg/g and 30 μg/g, respectively. Despite the lack of systematics in whole rock Li concentrations, Li contents of amphiboles in the KX amphibolite country rocks decrease systematically with distance from the KX pegmatite (Figure 3), while the major element

composition of the amphiboles remains more-or-less constant (Table S4 in Text S1).

[33] Similar to Li concentration, the whole rock δ^7Li of the KX pegmatite sample, +10.2, is unlikely to represent the δ^7Li of the whole KX pegmatite, which should be dominated by the spodumene. The spodumene has a δ^7Li value of +1.5, which we take as representative of the Li in the pegmatite.

[34] δ^7Li decreases systematically in the schists that crop out to the left (west) of the KX pegmatite (Figure 3), varying from −0.8 at ~0.15 m from the contact to ~−8.0 in the farthest schist at ~10 m. On the right (east) side of the KX contact, the trend in δ^7Li within the country rocks is gentler and is marked by two humps: one within quartzites at ~5 to 10 m distance from the contact of KX, the other within amphibolite at ~15 to 25 m from the contact. On this side of the pegmatite, the δ^7Li value shows an irregular decrease from +2 to +5 at the contact to ~−7 in the farthest amphibolite at ~ 31 m. The quartzo-feldspathic vein (δ^7Li = −0.5) does not appear to influence the δ^7Li values of its surroundings.

4.2. Animikie Red Ace Profile

[35] Li concentrations in the ARA pegmatites vary greatly. Two pegmatite samples, one quartz-rich and one tourmaline-rich from P1 have Li concentrations of 150 and 670 μg/g, respectively. The pegmatite sample from P2 has a Li concentration of 170 μg/g. Like the KX pegmatite, the coarse grain size of the ARA pegmatites make obtaining a representative sample difficult. In the ARA country rocks, Li concentrations decrease in an irregular fashion with distance away from the pegmatite (P1) contact up to ~30 m (Figure 4). Closer to the P2 pegmatite, within the amphibolite, Li concentration does not show any obvious trend, but remains substantially higher than in the regional amphibolites.

[36] The δ^7Li values in the ARA pegmatites do not vary significantly. The two P1 pegmatite samples have δ^7Li of +5.6 and +7.7, respectively. Similarly, the P2 pegmatite has δ^7Li of +7.0. Like the KX profile, δ^7Li in the ARA country rocks show a general decrease with distance from the pegmatite (P1) contact, from ~+4 and ~+6 in the country rocks near the contact, to −3.0 at ~45 m from the P1 contact (Figure 4). The δ^7Li values then increase slightly toward the P2 pegmatite.

4.3. Regional Samples

[37] Li concentrations in the regional schist and amphibolite samples range from 17 to 50 μg/g and

15 to 20 μg/g, respectively, which are typical of published data for schists and amphibolites [*Teng et al.*, 2004, 2006a]. Except for two extreme values (−6.1 and +6.7), δ^7Li values in these regional schists and amphibolites range from +0.7 to +2.8, which is similar to typical upper continental crustal values [*Teng et al.*, 2004]. By contrast, the schist and amphibolite country rocks from both the KX and ARA profiles generally have greater than 100 μg/g Li and δ^7Li that varies from −8 to +6.

5. Modeling Methods

[38] We have used both 1-D diffusion and 2-D advection-diffusion models to investigate the behavior of Li in the country rocks of the pegmatites. We provide details of these models in the auxiliary material.

[39] It has been demonstrated experimentally and empirically that Li isotopes will fractionate between minerals and fluid at the temperatures of pegmatite crystallization (e.g., 400 to 700°C) [*Teng et al.*, 2006b; *Wunder et al.*, 2006, 2007]. On the basis of Wunder et al.'s results, the fluid is isotopically heavier than either Li-mica or spodumene, and a similar sense of fractionation is expected between fluid and mineral for minerals in which Li is octahedrally coordinated. Such minerals (e.g., amphiboles, micas, spodumene) are the main hosts for Li in both the pegmatites and the country rocks. Although the fractionation factors, α, between different minerals and fluid are not the same, we assume the isotopic fractionation between the pegmatite and fluid approximates that between country rocks and fluid. Accordingly, we have not included any fluid-rock isotopic fractionation in the modeling.

5.1. One-Dimensional Diffusion Modeling

[40] A 1-D diffusion model, without advection, has been used to explain Li elemental and isotopic distributions in contact aureoles from previous case studies, such as those of *Teng et al.* [2006a] and *Marks et al.* [2007]. In this model, Li diffuses through a stagnant, grain-boundary fluid. According to Fick's law of diffusion, the solution for concentration as a function of time and distance for 1-D semi-infinite diffusion is

$$\frac{C_x - C_1}{C_o - C_1} = \text{erfc}\left(\frac{x}{2\sqrt{Dt}}\right),\qquad(1)$$

where x is the distance from the contact, C_x is the concentration at distance x from the contact, C_0 is the

concentration at the contact, C_1 is the concentration in unaffected country rocks, D is the diffusion coefficient, t is the duration of the diffusion process and erfc is the complementary error function. The characteristic length for diffusion (characteristic diffusive transport distance) is given as $2\sqrt{Dt}$. We have calculated a 1-D diffusion profile using the curve fitting tool of Matlab® to find the characteristic length of diffusion that best fits the geochemical observations for the KX profile. We did not calculate a 1-D model for the ARA profile, as neither the concentration nor isotopic data show the smooth trends that are expected for a 1-D model [e.g., *Teng et al.*, 2006a].

[41] For the KX model, we assume the pegmatite intruded at the left boundary of the 1-D country rock domain. We treat ^{7}Li and ^{6}Li as two different elements to model ^7C_x and ^6C_x separately and then calculate Li concentration and δ^7Li distribution as a function of distance. Therefore, we need to know δ^7Li as well as Li concentrations in the pegmatite and unaffected country rocks (regional average). A Li concentration of 400 μg/g in the KX pegmatite is used as the left boundary condition, C_0, in the modeling, because Li concentration of amphibole in amphibolite (1.1 m) from the nearest KX contact is 360 μg/g. This concentration is most likely to be a minimum value for the bulk pegmatite melts, because KX is a spodumene-amblygonite bearing pegmatite. Bulk Li concentration in this type of pegmatite is, on average, around 7000 μg/g [*Stewart*, 1978] but can exceed 9000 μg/g [*London*, 2008]. The unaffected country rocks are represented by the regional samples, so C_1 is the average concentration of the regional schist and amphibolite samples (27 μg/g). C_x can be calculated at different distances from the contact. As spodumene is the main Li carrier for the pegmatite, we adopt its δ^7Li as representative of the KX pegmatite. The average δ^7Li of +1.2 in regional schist and amphibolite samples is adopted as the original country rock value. With the determined characteristic length $2\sqrt{Dt}$, C_x can be calculated at different distances from the contact.

5.2. Advection-Diffusion Modeling

[42] In this model, the chemical distribution of Li in the country rock is governed by advective-diffusive transport of Li in a percolating pore fluid. The percolation of the pore fluid is driven by pressure gradients, which are caused by the increase in pore pressure triggered by intrusion of pegmatites into the fluid-saturated country rocks [*Ferry*, 1994, and references therein], and the buoyancy difference

Table 4. Boundary Conditions and Parameters in Different Cases[a]

Profile	Pressure (Pa)	[Li] (μg/g)	δ^7Li (‰)	Peclet	Beta	Grids
KX	$P_L = 2 \times 10^4(y + 1.5)$ $P_R = 2 \times 10^4 y$ $P_T = 0$ Pa, $P_B = 5 \times 10^4$	$C_L = 400$ $C_R = 79$ $C_T = C_B = 27$	$(\delta^7\text{Li})_L = +1.5$ $(\delta^7\text{Li})_R = -6.6$ $(\delta^7\text{Li})_T = (\delta^7\text{Li})_B = +1.2$	5.0	0.12	70×70
ARA	$P_L = 2 \times 10^4(y + 0.5)$ $P_R = 2 \times 10^4(y + 0.03)$ $P_T = 0$ Pa, $P_B = 3 \times 10^4$	$C_L = 500$ $C_R = 200$ $C_T = C_B = 27$	$(\delta^7\text{Li})_L = +5.0$ $(\delta^7\text{Li})_R = -1.0$ $(\delta^7\text{Li})_T = (\delta^7\text{Li})_B = +1.2$	2.5	0.12	80×80

[a]P and C are pressure and Li concentration, respectively. Subscripts L, R, T, and B represent left, right, top, and bottom boundary of parameters; y ranges from 0 (top) to 1 (bottom). Grid indicates the number of grids in the 1×1 2-D modeling domain.

between fluid and rock. The diffusion of Li isotopes is driven by the chemical potential gradient of Li in the pore fluid and the country rock. In this model, we assume the process is isothermal.

[43] The 2-D two-phase fluid flow model simulates percolation of Li-rich fluid flow from vertical pegmatite dikes into their adjacent porous country rocks with constant permeability in a rectangular domain. Although the influence of the smaller pegmatite (P2) in the ARA profile appears to be smaller than the larger pegmatite (P1), both intrusions are considered in the model. The consideration of a secondary pegmatite is an advantage of 2-D numerical model over the 1-D semi-infinite diffusion model.

[44] Percolation of a physically and chemically distinct fluid phase through a porous matrix is governed by coupled mass and momentum conservation of both the fluid and the matrix phases. These governing equations of two-phase viscous flow are presented in a number of studies [e.g., *Bercovici et al.*, 2001; *Connolly and Podladchikov*, 1998; *Drew and Passman*, 1999; *Hier-Majumder et al.*, 2006; *Ricard et al.*, 2001; *Richter and McKenzie*, 1984; *Scott and Stevenson*, 1984].

[45] The procedure for each case is as follows: Difference in pressure profiles are solved based on prescribed pressure along the horizontal and vertical boundaries. Velocity profiles are then solved from the difference in the pressure profile, using a Darcy flow relation. The two Li isotopes, ^{7}Li and ^{6}Li, are then treated as two different elements, and solved separately from advection-diffusion concentration solvers. Finally, Li concentration and δ^7Li profiles are calculated.

[46] Details of the governing equations and discussions of boundary conditions are provided in Text S1, section 1. Details of the numerical model and benchmarks are given by X.-M. Liu (University of Maryland, Advection-diffusion controlled Li isotopic fractionation in contact aureoles: A case

study from Florence County pegmatites, Wisconsin, 2009, available at http://www.lib.umd.edu/drum/handle/1903/9856). Boundary conditions for pressure, concentration, and δ^7Li of the KX and the ARA profiles are reported in Table 4 and displayed in Figure S3 in Text S1.

[47] The Peclet number (Pe) is the ratio of the magnitude of advection to diffusion, mathematically defined as

$$Pe = \frac{V_o L}{D_o} \qquad (2)$$

where V_o is the magnitude of the fluid advection velocity, expressed as

$$V_o = \frac{K \Delta \rho g}{\eta_f} \left(\frac{1 - \varphi}{\varphi} \right)$$

L is the characteristic length for diffusion, and D_o is the diffusion coefficient of Li isotopes.

[48] We need to determine values for the porosity (φ) and permeability of the country rock (K), density difference between fluid and solid ($\Delta\rho$), characteristic length (L), dynamic viscosity of fluids in porous rocks (η_f) and effective diffusion coefficients of Li isotopes (D_o) to calculate Pe. These parameters are discussed below.

[49] The permeability of porous rocks is dependent on their depths. *Manning and Ingebritsen* [1999] suggest the following permeability and depth relationship, after considering the permeability values inferred from thermal modeling and metamorphic systems: $\log K = -3.2 \log (y) - 14$, where y is depth in km and K is the corresponding permeability in m^2. Thus, if we assume a pegmatite intrusion depth of ~10–11 km [*Holm et al.*, 2005], we obtain an estimated permeability of $10^{-17.2}$ m^2. Considering the uncertainty of the relationship, a permeability range of 10^{-16}–10^{-18} m^2 is adopted here for estimating the value of the Peclet number. The estimated porosity of the country rocks is taken from *Connolly* [1997], who found 10^{-3} to 10^{-4} based on modeling of

metamorphism in a contact aureole. This range is used in calculation of the Peclet number in the numerical modeling. The characteristic length is determined according to the scale of modeling domain. For example, the characteristic length is ∼ 60 m in the ARA profile, which is the observed distance between the two pegmatites. Dynamic viscosity is a measure of resistance of a fluid deformed by either shear or extensional stress. A representative value of dynamic viscosity of water at ∼10 km is ∼$1.5 × 10^{-4}$ Pa s [*Walther and Orville*, 1982]. The dynamic viscosity of fluids in porous rocks, η_f, should have a similar value. The diffusion coefficient of Li through pure water at 25°C has been determined to be ∼10^{-9} m^2/s [*Li and Gregory*, 1974], which should be a minimum for our study, considering the significantly higher temperatures of the fluids involved in Li transport through the country rocks. Currently, there is no direct measurement of the effective Li diffusion coefficient in water-saturated metamorphic rocks. However, *Teng et al.* [2006a] estimate a minimum of $2 × 10^{-8}$ m^2/s for grain boundary diffusion of Li in amphibolite country rocks from the Tin Mountain pegmatite. They also found that the effective Li diffusion coefficient is ∼10 times larger in schist compared to the value in amphibolite country rocks. Thus, values of 10^{-8}–10^{-7} m^2/s are used to estimate the Peclet number.

[50] Combining the parameters given above with the estimate of the difference between the lithostatic and hydrostatic gradients $\Delta\rho g$ = ∼$1.7 × 10^4$ − 2.0 × 10^4 Pa m^{-1} [*Ague*, 2003], the Peclet number is loosely constrained to be 0 to $1 × 10^4$. We adopt *Pe* numbers of 5.0 and 2.5 for the KX and ARA profiles, respectively, which represent the best fit to the data. The diffusion only case, where *Pe* is equal to zero, is also considered in the modeling.

[51] Li isotopes diffuse at different rates. According to *Richter et al.* [1999], the ratio of the effective diffusion coefficients of the isotopes ^{6}Li and ^{7}Li are as follows: $D_6/D_7 = (m_7/m_6)^\beta$, where β is an empirical parameter to be determined from experimental data and m_7 and m_6 are the atomic masses of ^{7}Li and ^{6}Li. *Richter et al.* [2003] found that β is 0.215 for Li diffusion between basalt and rhyolite melts. For water, β is considered to be low, 0.015 and 0.071 (*Richter et al.* [2006] and *Fritz* [1992], respectively). *Teng et al.* [2006a] found a best fit β of 0.12, intermediate between that seen in water and magma, based on 1-D diffusion in amphibolite country rocks. We therefore adopt this value here, but investigate the effects of allowing β to vary from 0.02 to 0.2 (e.g., Figure S5 in Text S1 shows

that the magnitude of the δ^7Li anomaly increases with increasing β, but that the overall pattern remains the same).

[52] To compare the results of the numerical modeling with the analytical solution of 1-D diffusion from the equation (1) in section 5.1, we carry out two numerical experiments for ^{6}Li and ^{7}Li with no vertical variation (d/dy = 0) in the governing equations (7) and (8) in Text S1, section 1. The results of the numerical model are shown by the green curves in Figure 5 and the details are given in Text S1, section 2.

# 6. Modeling Results

6.1. One-Dimensional Modeling Results

[53] The results of the 1-D diffusion model are presented in Figure 5, where both Li concentration and δ^7Li are plotted as a function of distance from the contact between the KX pegmatite and its country rocks. Both Li concentration and δ^7Li show smooth decreasing trends from the left contact to the right. The calculated Li concentration profile matches the observed variation in amphibole Li content well. By contrast, the calculated δ^7Li profile shows a smooth decrease with distance from the pegmatite that matches the overall trend in the data, but not the detailed variations that are observed.

6.2. Two-Dimensional Modeling Results

[54] Results of the 2-D fluid flow advection-diffusion models are presented for both the KX and ARA profiles, following the numerical methods described above. Boundary conditions and parameters used in these models are given in Table 4. In addition, the influence of varying parameters is evaluated in Figures S4–S7 in Text S1.

6.2.1. King's-X Profile

[55] Pressure, fluid velocity, Li concentration and δ^7Li profiles for country rocks adjacent to the KX pegmatite intrusions are shown in Figure 6. Pressure increases vertically and there is a horizontal pressure gradient from the pegmatite intrusion into the country rock. Boundary effects are prominent at the upper-left and lower-right corners of the modeling domain for fluid velocity, due to the pressure gradients induced by the boundary conditions. Thus, caution needs to be taken when examining the results near the upper and bottom boundaries. Except for the regions that are close to
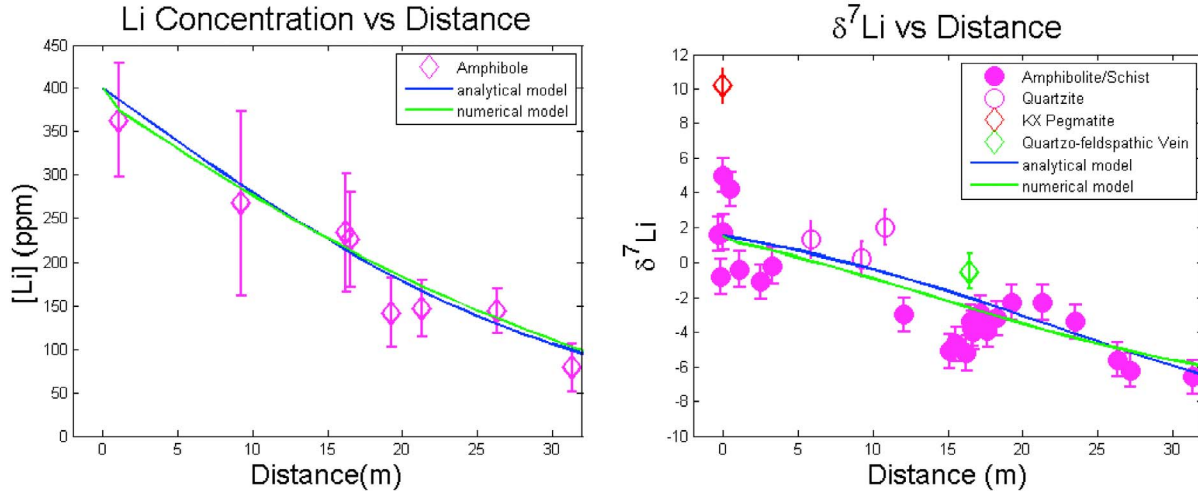
Figure 5. The 1-D diffusion models of (left) Li concentration and (right) δ^7Li versus distance plots for the KX profile. Blue lines indicate results from analytical solutions, and green lines are results from the numerical solutions. The characteristic length ($2\sqrt{Dt}$) is 34 m for both analytical and numerical solutions. The one-dimensional numerical solution was obtained for $Pe = 0$, following the methods discussed in section 5.2. The δ^7Li of the pegmatite is assumed to be the same as for spodumene.

the boundaries, fluid flows vertically due to its buoyancy. There is also a relatively weaker horizontal fluid flow from the pegmatite on the left boundary into the country rock. Concentration and δ^7Li distributions solved from the corresponding pressure and velocity field show Li concentration and isotopic composition distribution of the contact aureole at steady state conditions.

6.2.2. Animikie Red Ace Profile

[56] Pressure, fluid velocity, Li concentration and δ^7Li distributions for country rocks adjacent to the ARA pegmatites are shown in Figure 7. Pressure increases vertically and there are different horizontal pressure gradients from the two pegmatite intrusions. A stronger pressure gradient is prescribed to the P1 pegmatite under the assumption that P1 and P2 intruded simultaneously, and the exposure widths of the pegmatites track pressure gradients (P1 is about four times wider than P2). Theoretically, the fluid flows vertically due to its buoyancy and horizontally from the pegmatites on both left and right boundaries to the center of the country rock domain. However, the influence of the pegmatite on the left is much larger compared to the one on the right (Table 4), due to the prescribed pressure differences, which gives rise to an overall fluid flow direction from left to right. Like the KX profile, numerical artifacts are prominent at the upper-left and lower-right corners of the modeling domain

due to the prescription of boundary conditions and caution then needs to be taken when examining the distributions in these areas. Concentration and δ^7Li distributions solved from the corresponding pressure and velocity field are all shown at steady state conditions. As expected from the prescribed conditions, all results show that the influence of the pegmatite on the left (P1) is greater than the pegmatite on the right (P2).

6.3. Controlling Parameters

[57] A prime objective of this study is to offer insights on the most important processes controlling Li elemental and isotopic distribution in metamorphic contact aureole settings. According to the definition of the Peclet number, we know that it includes many parameters, such as porosity and permeability of the country rock, vertical pressure gradient, characteristic length, dynamic viscosity of fluids in porous rocks and effective diffusion coefficients of Li isotopes. Our modeling results show that the Peclet number plays an important role in controlling both Li concentration and δ^7Li distribution in the model. (Figures S4–S7 in Text S1 illustrate the influence of the Peclet number, β value, Li concentration and δ^7Li boundary conditions in the 2-D advection-diffusion modeling.) The β value influences the magnitude of the δ^7Li anomalies, but does not influence Li concentration distributions. By contrast, parameters that define the boundary conditions, such as Li concentrations
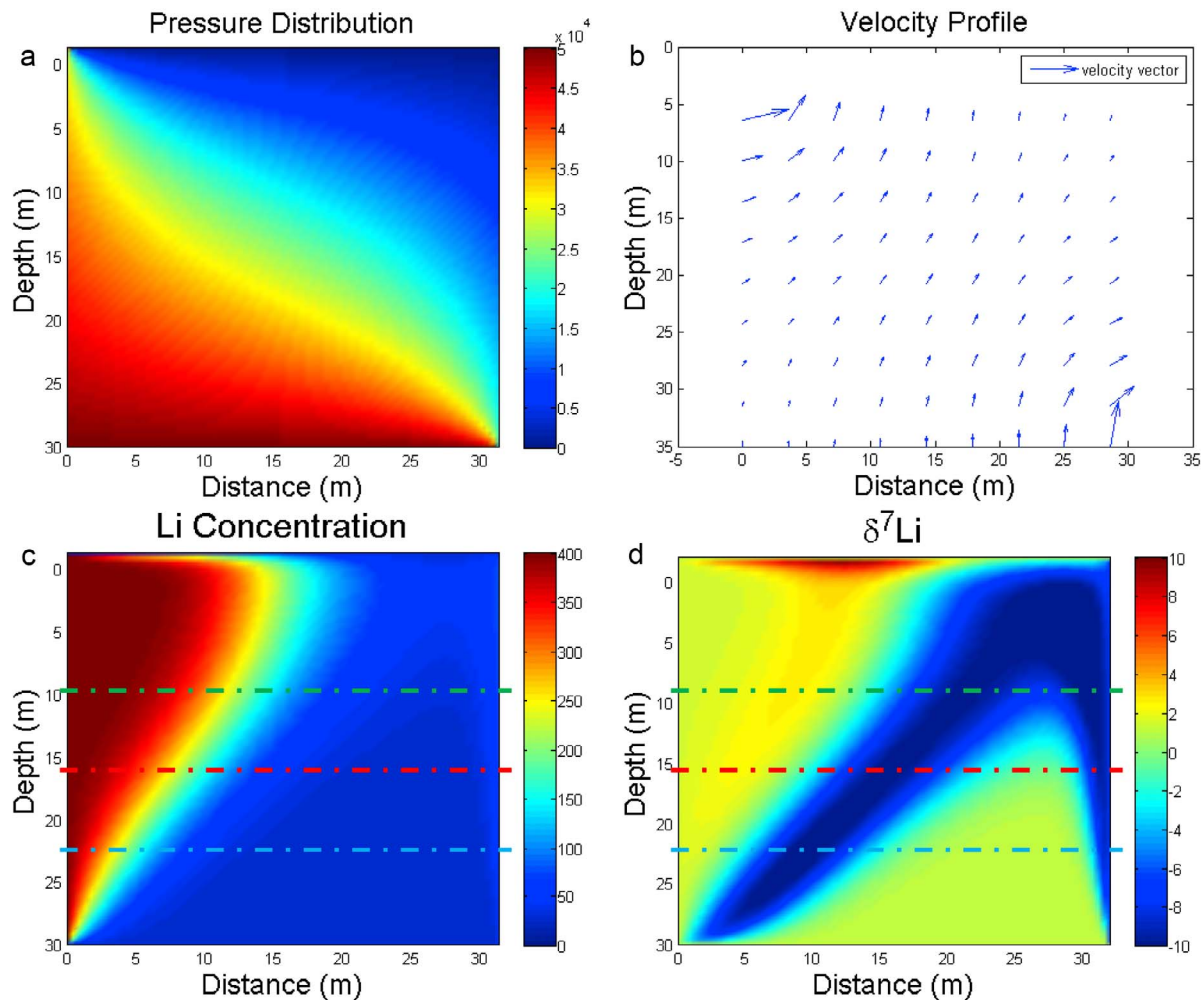
Figure 6. Steady state 2-D modeling results for the KX profile with constant permeability. (a) Pressure distribution (in Pa). (b) Fluid velocity field, where the size of the arrows is proportional to the fluid velocity. (c) Li concentration distribution (in μg/g). $Pe = 5.0$. (d) The δ^7Li distribution (in ‰); $\beta = 0.12$. Model grid is 70 × 70 cells. Dashed lines in Figures 6c and 6d indicate horizontal cross-section lines at different depths (9, 16, and 22 m).

and δ^7Li values, do not have much influence on the Li concentration and δ^7Li distributions when allowed to vary within reasonable bounds.
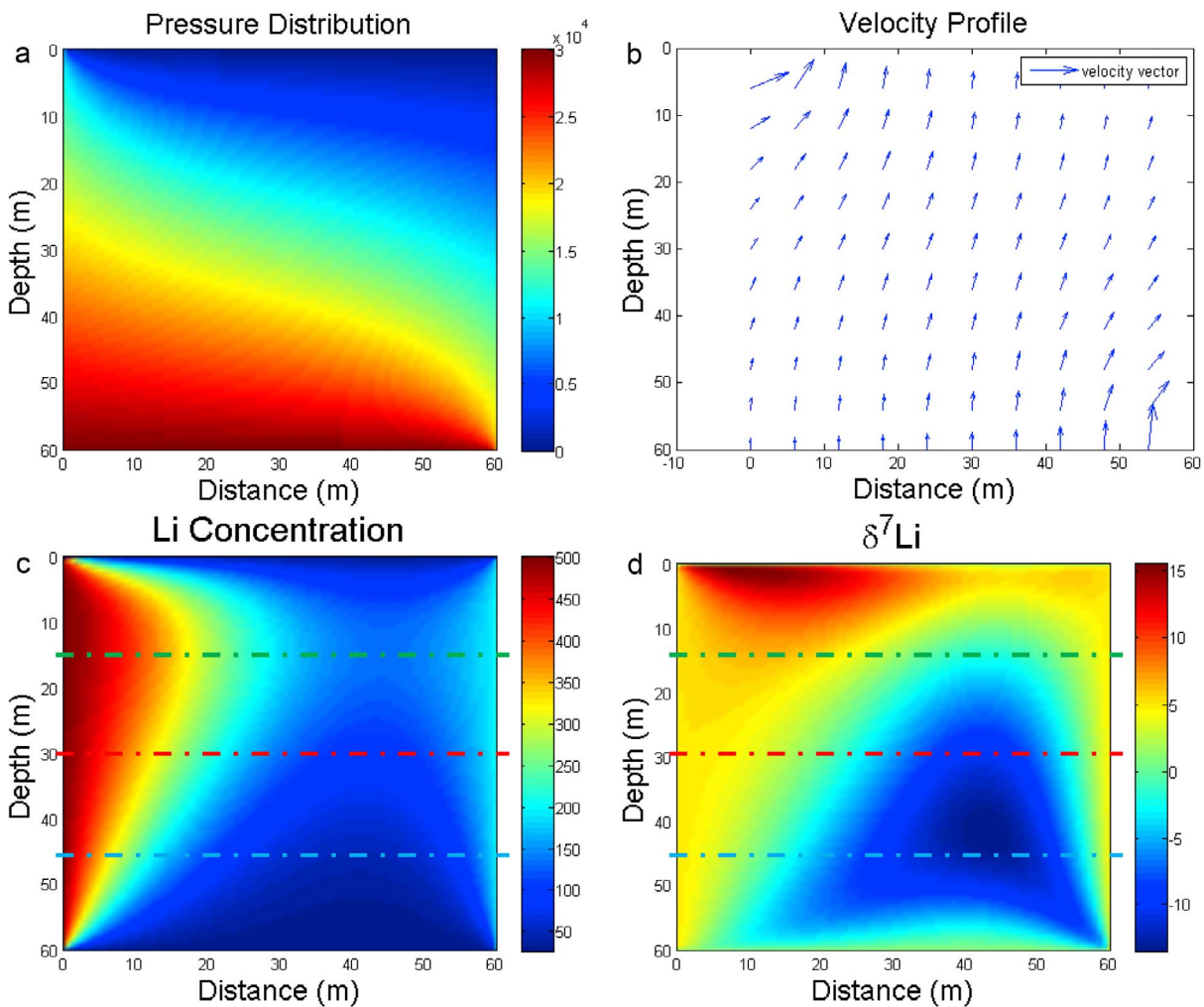
7. Discussion

[58] We now combine the results from Li analyses and modeling in order to elucidate the mechanisms that control Li distribution in contact aureoles.

[59] While dehydration reactions may influence the Li distribution in country rocks of contact aureoles [*Teng et al.*, 2007], no evidence for dehydration from either the field or thin-sections was found in this study. Furthermore, several studies have shown that metamorphic dehydration has a minor effect, if

any, on the δ^7Li of metapelitic rocks [*Qiu et al.*, 2009; *Teng et al.*, 2007]. Thus, metamorphic dehydration is unlikely to control the Li distribution in the KX or ARA profiles.

[60] The marked enrichment of Li in the country rocks of both the KX and ARA profiles relative to regional samples (Figures 6 and 7) reflects the influence of the pegmatites on the country rocks. Moreover, the decrease in δ^7Li with increasing distance away from both the KX and ARA pegmatite contacts is consistent with kinetic isotope fractionation produced as Li diffused from the pegmatites into the country rocks. Similar observations for the country rocks of the Tin Mountain pegmatite led *Teng et al.* [2006a] to suggest Li diffusion occurred through a grain-boundary fluid.

Geochemistry
Geophysics
Geosystems

G^3

LIU ET AL.: LITHIUM IN CONTACT AUREOLES

10.1029/2010GC003063

Figure 7. Steady state 2-D modeling results for the ARA profile with constant permeability. (a) Pressure distribution (in Pa). (b) Velocity field, where the size of the arrows is proportional to the fluid velocity. (c) Li concentration distribution (in $\mu g/g$). $Pe = 2.5$. (d) The δ^7Li distribution (in ‰); $\beta = 0.12$. Model grid is 80×80 cells. Dashed lines in Figures 7c and 7d indicate horizontal cross-section lines at different depths (15, 30, and 45 m).

[61] Two lines of evidence suggest an important role for fluids in transporting Li from the Wisconsin pegmatites into the country rocks. First, Li concentrations of amphiboles in amphibolite country rocks show a prominent trend of decreasing concentration with distance away from the KX contact on the tens of meters scale (Figure 1). Assuming that the partition coefficient of Li between amphiboles and fluid is constant, this trend suggests the equilibration of the amphiboles with Li-rich grain boundary fluids derived from the pegmatite. Second, the KX country rocks contain secondary minerals, such as chlorite, fluorite and tourmaline, especially within the first few meters of the pegmatite contact (Table S1 in Text S1). This also suggests infiltra-

tion of fluids from the pegmatite into the country rocks accompanying pegmatite intrusion.

7.1. King's-X Profile

[62] The Peclet number (Pe) can be used to quantify the effect of the magnitude of diffusion versus advection on Li in this profile. Pe goes to infinity if there is no diffusion and Pe is equal to zero if there is only diffusion and no advection. Thus, Pe varies between zero and infinity.

[63] For the 1-D diffusion model ($Pe = 0$) a characteristic length ($2\sqrt{Dt}$) of ~34 m and a β value of 0.06 are found to provide the best fit to the profile data (see Figure S8 in Text S1). This model, shown

in Figure 5, can explain the Li concentration distribution, but it does not reproduce the irregular distribution of δ^7Li through the country rocks.

[64] To compare the δ^7Li distributions from 2-D numerical modeling (Figure 6) with geochemical observation (Figure 3), Li concentration and δ^7Li distributions need to be converted to 1-D distributions, as every horizontal line on the 2-D distribution is a 1-D δ^7Li profile. To reflect the vertical variations, 1-D δ^7Li distributions are shown at three different depths (9, 16, and 22 m – marked by horizontal lines on Figures 6a and 6d), which encompass the mid-depth of the modeling domain and avoid the boundary effects in the upper left and lower right corners of the domain. In reality, the sampling transverse lines may not be exactly perpendicular to the contact and the contact may not be flat, which may account for some of the irregularities in the geochemical data.

[65] The resulting 1-D representation of the 2-D advection-diffusion model (with Pe = 5.0) for the KX profile (Figure 8) show multiple humps, as observed in the δ^7Li of the profile, but the model does not provide a good match to the geochemical data, especially close to the contact. Moreover, the 1-D diffusion model seems to explain the Li concentration distribution of the KX profile better.

[66] As shown above, neither 1-D diffusion nor 2-D advection-diffusion with constant permeability can explain the observed Li elemental and isotopic distributions well. There are several potential reasons for the mismatches between models and observations, including (1) lithological variations in country rocks, (2) 3-D fluid flow that cannot be modeled by the 1-D and 2-D methods employed here, and (3) intervening subsurface dikes that are not exposed in the outcrops. For example, the hump in δ^7Li at around 5 to 10 m distance from the KX profile may reflect lithology (quartzite), since quartz is known to be isotopically heavy [*Teng et al.*, 2006b]. Moreover, it is possible (and probably likely) that the irregularities of the lithium isotopic distribution are the result of heterogeneous fluid flow caused by permeability variations in the country rocks, which implies that fluid advection occurred.

[67] The very long transport length observed for Li compared to its diffusion coefficient in water is evidence in support of fluid advection within the country rocks. If one assumes that only diffusion occurs, the diffusion coefficient of Li can be estimated from the characteristic length scales of diffusion and the cooling time of the pegmatite dikes. *Sirbescu et al.* [2008] estimated that a 2.5 m wide

pegmatite such as the ARA cools from its liquidus temperature of ~720°C to its solidification temperature of <400°C in less than 50 days if it intrudes country rocks that are ~500°C colder than the magma. The characteristic length of diffusion in the KX profile is at least 30 m. These time and scale constraints imply a minimum Li diffusion coefficient of 2×10^{-4} m^2/s, which is three to four orders of magnitude faster than expected for Li diffusion in water at 0.3 GPa and temperatures between 25°C and 700°C [*Bourg and Sposito*, 2007; *Li and Gregory*, 1974; *Oelkers and Helgeson*, 1988]. There are two end-member explanations for the unreasonable high diffusion coefficient of Li: (1) Li transport into the country rock via advection in addition to diffusion; and (2) continuous fluid flow and Li diffusion after pegmatite crystallization. Both explanations are considered likely. Combined with the irregularities of the lithium isotopic distribution in the country rocks, we can conclude that advection not only occurs, but also is essential for Li transport in the country rocks.

7.2. Animikie Red Ace Profile

[68] Like the KX profile, Li concentrations in the country rocks of the ARA profile decrease, but do not show simple trends with distance away from the two bordering pegmatites. Also, like the KX profile, amphibolite and schist country rocks adjacent to the ARA pegmatites have much higher Li concentrations compared to their regional counterparts. Both the large Li concentration difference between country rocks and regional samples and the δ^7Li distribution indicate that the ARA pegmatite on the left side (P1) has largely influenced the Li distribution in its country rocks. By contrast, the influence of the smaller ARA pegmatite on the right appears to be small. This may be due to its smaller size, as inferred on the basis of our modeling, a lower Li concentration in the P2 magma, or P2 pegmatite emplacement prior to the P1 pegmatite, so that the latter obscured some of the influence of the P2 pegmatite on the country rocks.

[69] Like the KX models, 1-D Li and δ^7Li slices are illustrated at three different depths (15, 30 and 45 m) through the ARA profile (Figure 9), which encompass the mid-depth of the modeling domain. At any single depth, the model does not match the distribution of Li isotopic composition along the profile well, and the misfit is especially severe close to the ARA pegmatite intrusions. As the country rock foliations are perpendicular to the exposure/ modeling plane and subparallel to the strike of the
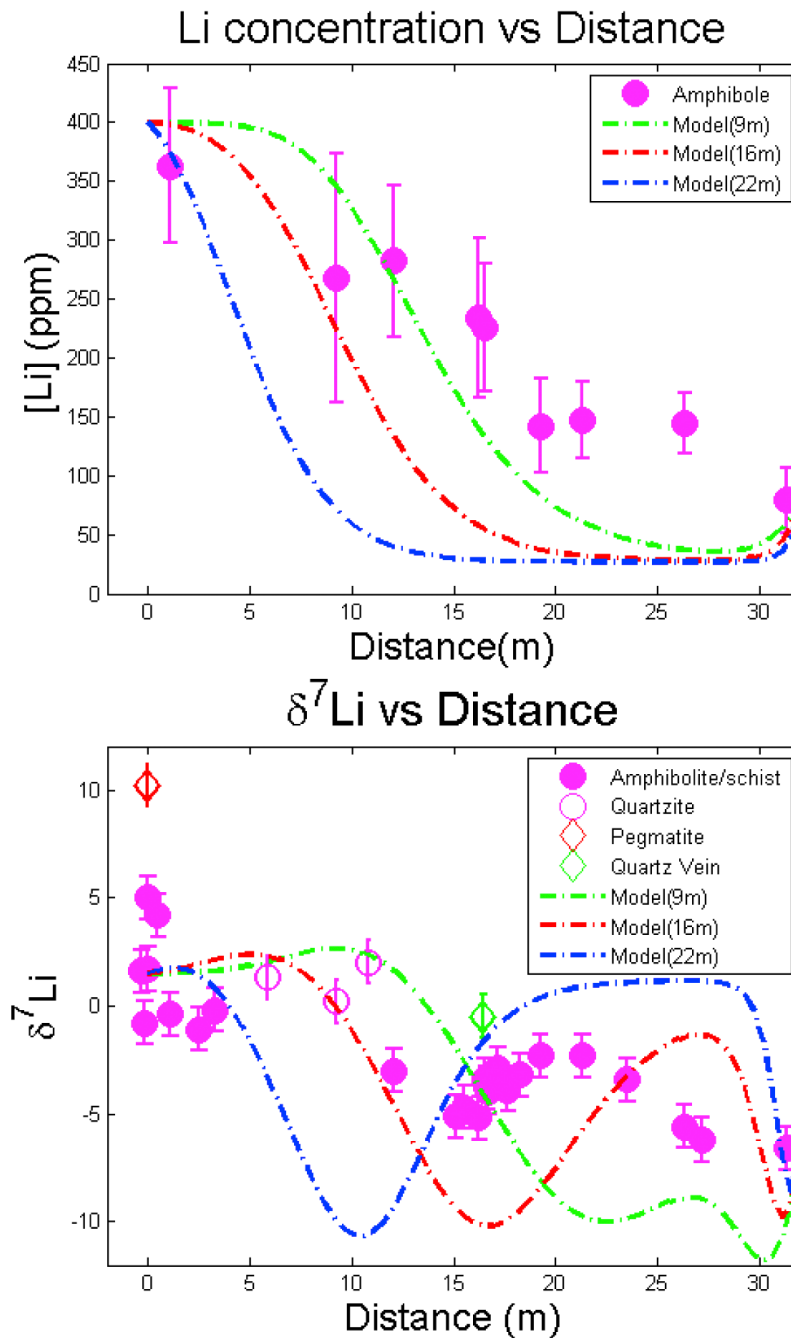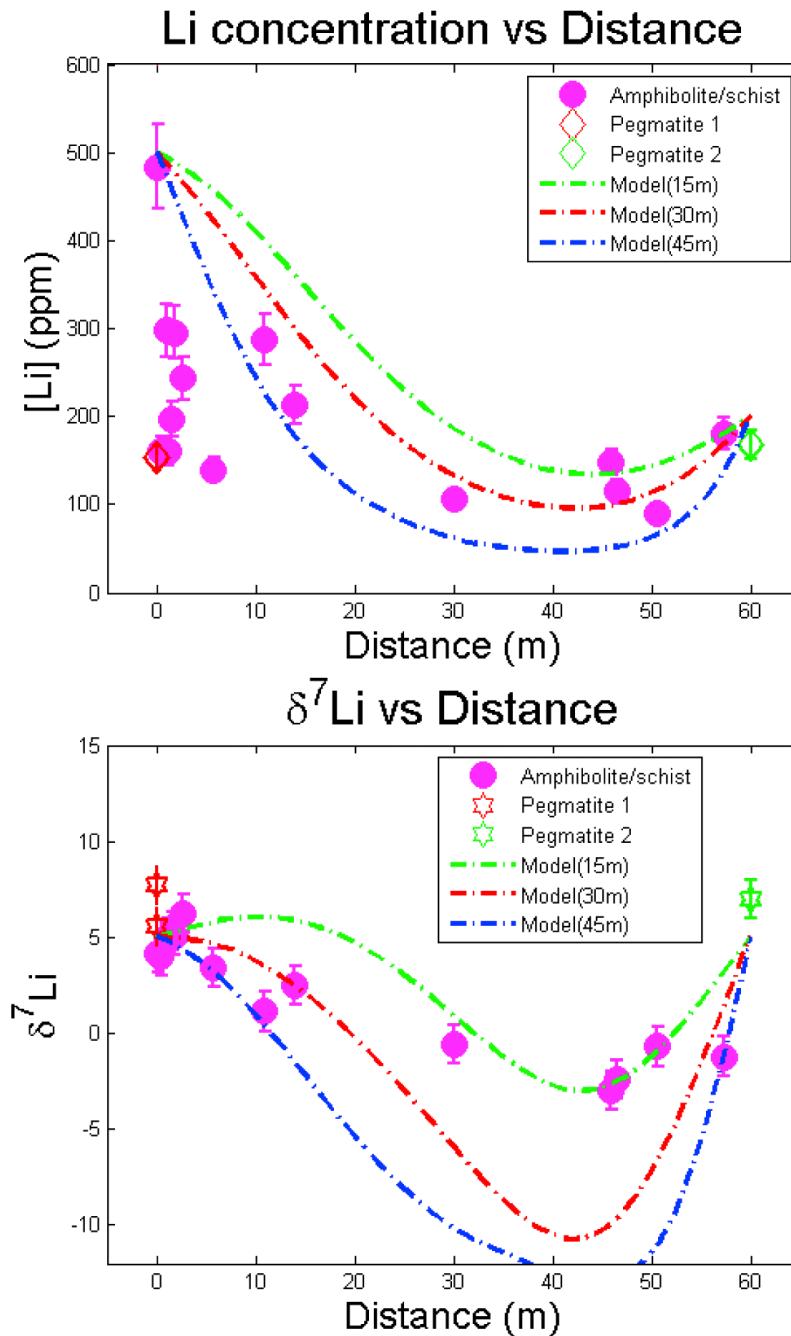
Figure 8. Combination of numerical solutions and geochemical observation for (top) Li concentration and (bottom) δ^7Li versus distance plots for the KX profile ($Pe = 5.0$). Curves are the 2-D modeling results from Figure 6 plotted for different depths (9, 16, and 22 m). Boundary conditions for [Li] and δ^7Li are 400 μg/g, +1.5 for the left contact and 79 μg/g, −6.6 for the right contact, respectively.

dike (Figure 2), the mismatches between the model and geochemical observations may be explained by heterogeneous permeability induced by this foliation within country rocks or intervening, hidden small dikes in the country rocks, assuming fluid advection. *Huenges et al.* [1997] suggest that permeability parallel to foliation is up to an order of

magnitude larger than permeability perpendicular to the foliation within the same rocks. The length scale of Li transport in this profile is even longer than for the exposed KX profile, leading to an even greater mismatch between the calculated diffusion coefficient for Li in water and those from the literature. This observation again supports an advective com-

Figure 9. Combination of numerical solutions and geochemical observation for Li concentration and δ^7Li versus distance plots for the ARA profile (Pe = 2.5). Curves are the 2-D modeling results from Figure 7 plotted for different depths (15, 30, and 45 m). Boundary conditions for Li concentration and δ^7Li are 500 μg/g, +5.0 for the left contact and 200 μg/g, −1.0 for the right contact, respectively.

ponent, in addition to diffusion, in producing the Li distribution in the country rocks.

[70] Both the KX and the ARA profiles indicate that Li is not only transported through diffusion, but also through advection via aqueous fluid. The different patterns of irregularity in Li elemental and isotopic distributions are likely caused by heterogeneous fluid flow induced by variable permeability. The reasons for the heterogeneous permeability may be different between the two profiles. For the KX profile, it is likely to be related to the variation of lithology in the country rocks, whereas, for the ARA profile, permeability heterogeneity variations

induced by heterogeneities in foliation is more likely.

8. Conclusions

[71] The pegmatite dikes in Florence County, Wisconsin, have had a large impact on the Li budget of their adjacent country rocks, with Li concentrations enriched by up to a factor of twenty over regional values. Furthermore, Li from the pegmatite has traveled more than 50 m into the country rocks. Systematic decreases in δ^7Li away from the pegmatites indicate that diffusion was responsible for at least part of this ingress of Li into the country rocks.

[72] Diffusion of Li in a stagnant grain-boundary fluid cannot explain the Li isotopic distribution in the country rocks, nor can simple 2-D advection-diffusion models. Moreover, the scale of Li transport, coupled with constraints on cooling rates suggests advection of fluids from the pegmatites into the country rocks. Compared to previous Li isotopic studies [e.g., *Teng et al.*, 2006a; *Marks et al.*, 2007], this study demonstrates that fluid infiltration accompanies diffusion of Li from the intrusions into heterogeneous country rocks. Permeability structure induced by lithological variation and/or foliation may have also played a role in the heterogeneous distribution of Li isotopes that is observed in the country rocks.

Acknowledgments

References

Ague, J. J. (2003), Fluid flow in the deep crust, in *Treatise on Geochemistry*, vol. 3, *The Crust*, edited by R. L. Rudnick, pp. 195–228, Elsevier-Pergamon, Oxford, U. K.

Baumgartner, L. P., and J. W. Valley (2001), Stable isotope transport and contact metamorphic fluid flow, in *Stable Isotope Geochemistry*, *Rev. Mineral. Geochem.*, vol. 43, edited by J. W. Valley and D. R. Cole, pp. 415–467, doi:10.2138/gsrmg.43.1.415, Mineral. Soc. of Am., Chantilly, Va.

Bercovici, D., Y. Ricard, and G. Schubert (2001), A two-phase model for compaction and damage: 1. General theory, *J. Geophys. Res.*, *106*(B5), 8887–8906, doi:10.1029/2000JB900430.

Bickle, M. J., and D. McKenzie (1987), The transport of heat and matter by fluids during metamorphism, *Contrib. Mineral. Petrol.*, *95*(3), 384–392, doi:10.1007/BF00371852.

Bourg, I. C., and G. Sposito (2007), Molecular dynamics simulations of kinetic isotope fractionation during the diffusion of ionic species in liquid water, *Geochim. Cosmochim. Acta*, *71*(23), 5583–5589, doi:10.1016/j.gca.2007.01.021.

Bowman, J. R., and S. D. Willett (1991), Spatial patterns of oxygen isotope exchange during one-dimensional fluid infiltration, *Geophys. Res. Lett.*, *18*(5), 971–974, doi:10.1029/91GL01079.

Brenan, J. M., E. Neroda, C. C. Lundstrom, H. F. Shaw, F. J. Ryerson, and D. L. Phinney (1998a), Behaviour of boron, beryllium, and lithium during melting and crystallization: Constraints from mineral-melt partitioning experiments, *Geochim. Cosmochim. Acta*, *62*(12), 2129–2141, doi:10.1016/S0016-7037(98)00131-8.

Brenan, J. M., F. J. Ryerson, and H. F. Shaw (1998b), The role of aqueous fluids in the slab-to-mantle transfer of boron, beryllium, and lithium during subduction: Experiments and models, *Geochim. Cosmochim. Acta*, *62*(19–20), 3337–3347, doi:10.1016/S0016-7037(98)00224-5.

Connolly, J. A. D. (1997), Devolatilization-generated fluid pressure and deformation-propagated fluid flow during prograde regional metamorphism, *J. Geophys. Res.*, *102*(B8), 18,149–18,173, doi:10.1029/97JB00731.

Connolly, J. A. D., and Y. Y. Podladchikov (1998), Compaction-driven fluid flow in viscoelastic rock, *Geodin. Acta*, *11*(2–3), 55–84, doi:10.1016/S0985-3111(98)80006-5.

Cook, S. J., J. R. Bowman, and C. B. Forster (1997), Contact metamorphism surrounding the Alta Stock: Finite element model simulation of heat- and ^{18}O/^{16}O mass-transport during prograde metamorphism, *Am. J. Sci.*, *297*(1), 1–55.

Cui, X. J., P. I. Nabelek, and M. Liu (2001), Heat and fluid flow in contact metamorphic aureoles with layered and transient permeability, with application to the Notch Peak aureole, Utah, *J. Geophys. Res.*, *106*(B4), 6477–6491, doi:10.1029/2000JB900418.

Cui, X. J., P. I. Nabelek, and M. A. Liu (2002), Numerical modeling of fluid flow and oxygen isotope exchange in the notch peak contact-metamorphic aureole, Utah, *Geol. Soc. Am. Bull.*, *114*(7), 869–882, doi:10.1130/0016-7606(2002) 114<0869:NMOFFA>2.0.CO;2.

Deming, D. (1994), Fluid flow and heat transport in the upper continental crust, *Geol. Soc. Spec. Publ.*, *78*(1), 27–42, doi:10.1144/GSL.SP.1994.078.01.04.

Drew, D., and S. Passman (1999), *Theory of Multicomponent Flow*, Springer, New York.

Falster, A. U., W. B. Simmons, and K. L. Webber (1996), The mineralogy and geochemistry of the animikie red ace pegmatite, Florence County, Wisconsin, *Recent Res. Dev. Mineral.*, *1*, 7–67.

Falster, A. U., W. B. Simmons, and K. L. Webber (2005), Origin of the pegmatites in the Hoskin Lake pegmatite field, Florence Co., Wisconsin, in *Crystallization Processes in Granitic Pegmatites, International Meeting in Cavoli, Elba Island, Italy, May 23–28, 2005*, edited by F. Pezzotta, Mineral. Soc. of Am., Chantilly, Va.

Ferry, J. M. (1994), A historical review of metamorphic fluid-flow, *J. Geophys. Res.*, *99*(B8), 15,487–15,498, doi:10.1029/94JB01147.

Ferry, J. M., B. A. Wing, S. C. Penniston-Dorland, and D. Rumble (2002), The direction of fluid flow during contact metamorphism of siliceous carbonate rocks: New data for the Monzoni and Predazzo aureoles, northern Italy, and a global review, *Contrib. Mineral. Petrol.*, *142*(6), 679–699.

Flesch, G., A. Anderson, and H. Svec (1973), A secondary isotopic standard for $^6Li/^7Li$ determinations, *Int. J. Mass Spectrom. Ion Phys.*, *12*(3), 265–272, doi:10.1016/0020-7381(73)80043-9.

Fritz, S. J. (1992), Measuring the ratio of aqueous diffusion-coefficients between $^6Li^+Cl$- and $^7Li^+Cr$- by osmometry, *Geochim. Cosmochim. Acta*, *56*(10), 3781–3789, doi:10.1016/0016-7037(92)90170-N.

Hier-Majumder, S., Y. Ricard, and D. Bercovici (2006), Role of grain boundaries in magma migration and storage, *Earth Planet. Sci. Lett.*, *248*(3–4), 735–749, doi:10.1016/j.epsl.2006.06.015.

Holm, D. K., W. R. Van Schmus, L. C. MacNeill, T. J. Boerboom, D. Schweitzer, and D. Schneider (2005), U-pb zircon geochronology of paleoproterozoic plutons from the northern midcontinent, USA: Evidence for subduction flip and continued convergence after geon 18 Penokean orogenesis, *Geol. Soc. Am. Bull.*, *117*(3), 259–275, doi:10.1130/B25395.1.

Huenges, E., J. Erzinger, J. Kuck, B. Engeser, and W. Kessels (1997), The permeable crust: Geohydraulic properties down to 9101 m depth, *J. Geophys. Res.*, *102*(B8), 18,255–18,265, doi:10.1029/96JB03442.

James, R. H., and M. R. Palmer (2000), The lithium isotope composition of international rock standards, *Chem. Geol.*, *166*(3–4), 319–326, doi:10.1016/S0009-2541(99)00217-X.

Li, Y. H., and S. Gregory (1974), Diffusion of ions in seawater and in deep-sea sediments, *Geochim. Cosmochim. Acta*, *38*(5), 703–714, doi:10.1016/0016-7037(74)90145-8.

London, D. (2008), Pegmatites, *Spec. Publ. Can. Mineral.*, *10*, 347.

Lundstrom, C. C., M. Chaussidon, A. T. Hsui, P. Kelemen, and M. Zimmerman (2005), Observations of Li isotopic variations in the trinity ophiolite: Evidence for isotopic fractionation by diffusion during mantle melting, *Geochim. Cosmochim. Acta*, *69*(3), 735–751, doi:10.1016/j.gca.2004.08.004.

Magna, T., U. H. Wiechert, and A. N. Halliday (2004), Low-blank isotope ratio measurement of small samples of lithium using multiple-collector ICPMS, *Int. J. Mass Spectrom.*, *239*(1), 67–76, doi:10.1016/j.ijms.2004.09.008.

Manning, C. E., and S. E. Ingebritsen (1999), Permeability of the continental crust: Implications of geothermal data and metamorphic systems, *Rev. Geophys.*, *37*(1), 127–150, doi:10.1029/1998RG900002.

Marks, M. A. W., R. L. Rudnick, C. McCammon, T. Vennemann, and G. Markl (2007), Arrested kinetic Li isotope fractionation at the margin of the Ilimaussaq complex, south Greenland: Evidence for open-system processes during final cooling of peralkaline igneous rocks, *Chem. Geol.*, *246*(3–4), 207–230, doi:10.1016/j.chemgeo.2007.10.001.

Moriguti, T., and E. Nakamura (1998), High-yield lithium separation and the precise isotopic analysis for natural rock and aqueous samples, *Chem. Geol.*, *145*(1–2), 91–104, doi:10.1016/S0009-2541(97)00163-0.

Norton, D., and H. P. Taylor (1979), Quantitative simulation of the hydrothermal systems of crystallizing magmas on the basis of transport-theory and oxygen isotope data: Analysis of the Skaergaard intrusion, *J. Petrol.*, *20*(3), 421–486.

Oelkers, E. H., and H. C. Helgeson (1988), Calculation of the thermodynamic and transport properties of aqueous species at high pressures and temperatures: Aqueous tracer diffusion coefficients of ions to 1000°C and 5 kb, *Geochim. Cosmochim. Acta*, *52*(1), 63–85, doi:10.1016/0016-7037(88)90057-9.

Pistiner, J. S., and G. M. Henderson (2003), Lithium-isotope fractionation during continental weathering processes, *Earth Planet. Sci. Lett.*, *214*(1–2), 327–339, doi:10.1016/S0012-821X(03)00348-0.

Qiu, L., R. L. Rudnick, W. F. McDonough, and R. J. Merriman (2009), Li and δ^7Li in mudrocks from the British Caledonides: Metamorphism and source influences, *Geochim. Cosmochim. Acta*, *73*(24), 7325–7340, doi:10.1016/j.gca.2009.08.017.

Ricard, Y., D. Bercovici, and G. Schubert (2001), A two-phase model for compaction and damage: 2. Applications to compaction, deformation, and the role of interfacial surface tension, *J. Geophys. Res.*, *106*(B5), 8907–8924, doi:10.1029/2000JB900431.

Richardson, P. J. (1998), The mineralogy and geochemistry of the King's-X pegmatite in Florence County, Wisconsin, Master's thesis, 134 pp., Univ. of New Orleans, New Orleans, La.

Richardson, P. J., A. U. Falster, and W. B. Simmons (1995), HFSE mineralization associated with amblygonite-montebrasite crystallization in the King's-X pegmatite, Florence County, Wisconsin, paper presented at Geological Society of America Meeting, New Orleans, La.

Richter, F. M., and D. McKenzie (1984), Dynamical models for melt segregation from a deformable matrix, *J. Geol.*, *92*(6), 729–740, doi:10.1086/628908.

Richter, F. M., Y. Liang, and A. M. Davis (1999), Isotope fractionation by diffusion in molten oxides, *Geochim. Cosmochim. Acta*, *63*(18), 2853–2861, doi:10.1016/S0016-7037(99)00164-7.

Richter, F. M., A. M. Davis, D. J. DePaolo, and E. B. Watson (2003), Isotope fractionation by chemical diffusion between molten basalt and rhyolite, *Geochim. Cosmochim. Acta*, *67*(20), 3905–3923, doi:10.1016/S0016-7037(03)00174-1.

Richter, F. M., R. A. Mendybaev, J. N. Christensen, I. D. Hutcheon, R. W. Williams, N. C. Sturchio, and A. D. Beloso (2006), Kinetic isotopic fractionation during diffusion of ionic species in water, *Geochim. Cosmochim. Acta*, *70*(2), 277–289, doi:10.1016/j.gca.2005.09.016.

Rosner, M., L. Ball, B. Peucker-Ehrenbrink, J. Blusztajn, W. Bach, and J. Erzinger (2007), A simplified, accurate and fast method for lithium isotope analysis of rocks and fluids, and δ^7Li values of seawater and rock reference materials, *Geostand. Geoanal. Res.*, *31*(2), 77–88, doi:10.1111/j.1751-908X.2007.00843.x.

Rudnick, R. L., P. B. Tomascak, H. B. Njo, and L. R. Gardner (2004), Extreme lithium isotopic fractionation during continental weathering revealed in saprolites from South Carolina, *Chem. Geol.*, *212*(1–2), 45–57, doi:10.1016/j.chemgeo.2004.08.008.

Scott, D. R., and D. J. Stevenson (1984), Magma solitons, *Geophys. Res. Lett.*, *11*(11), 1161–1164, doi:10.1029/GL011i011p01161.

Sims, P., K. Schulz, and Z. Peterman (1992), Geology and geochemistry of Early Proterozoic rocks in the Dunbar area, northeastern Wisconsin, *U.S. Geol. Surv. Prof. Pap., 1517*, 65 pp.

Sirbescu, M. L. C., E. E. Hartwick, and J. J. Student (2008), Rapid crystallization of the Animikie Red Ace Pegmatite, Florence county, northeastern Wisconsin: Inclusion microthermometry and conductive-cooling modeling, *Contrib.*

Mineral. Petrol., *156*(3), 289–305, doi:10.1007/s00410-008-0286-0.

Sirbescu, M. L. C., M. A. Leatherman, J. J. Student, and A. R. Beers (2009), Apatite textures and compositions as records of crystallization processes in the Animikie Red Ace Pegmatite dike, Wisconsin, USA, *Can. Mineral.*, *47*, 725–743, doi:10.3749/canmin.47.4.725.

Stewart, D. B. (1978), Petrogenesis of lithium-rich pegmatites, *Am. Mineral.*, *63*, 970–980.

Teng, F. Z., W. F. McDonough, R. L. Rudnick, C. Dalpe, P. B. Tomascak, B. W. Chappell, and S. Gao (2004), Lithium isotopic composition and concentration of the upper continental crust, *Geochim. Cosmochim. Acta*, *68*(20), 4167–4178, doi:10.1016/j.gca.2004.03.031.

Teng, F. Z., W. F. McDonough, R. L. Rudnick, and R. J. Walker (2006a), Diffusion-driven extreme lithium isotopic fractionation in country rocks of the Tin Mountain pegmatite, *Earth Planet. Sci. Lett.*, *243*(3–4), 701–710, doi:10.1016/j.epsl.2006.01.036.

Teng, F. Z., W. F. McDonough, R. L. Rudnick, R. J. Walker, and M. L. C. Sirbescu (2006b), Lithium isotopic systematics of granites and pegmatites from the Black Hills, South Dakota, *Am. Mineral.*, *91*(10), 1488–1498, doi:10.2138/am.2006.2083.

Teng, F. Z., W. F. McDonough, R. L. Rudnick, and B. A. Wing (2007), Limited lithium isotopic fractionation during progressive metamorphic dehydration in metapelites: A case study from the Onawa contact aureole, Maine, *Chem. Geol.*, *239*(1–2), 1–12, doi:10.1016/j.chemgeo.2006.12.003.

Walther, J. V., and P. M. Orville (1982), Volatile production and transport in regional metamorphism, *Contrib. Mineral. Petrol.*, *79*(3), 252–257, doi:10.1007/BF00371516.

Wunder, B., A. Meixner, R. L. Romer, and W. Heinrich (2006), Temperature-dependent isotopic fractionation of lithium between clinopyroxene and high-pressure hydrous fluids, *Contrib. Mineral. Petrol.*, *151*(1), 112–120, doi:10.1007/s00410-005-0049-0.

Wunder, B., A. Meixner, R. L. Romer, A. Feenstra, G. Schettler, and W. Heinrich (2007), Lithium isotope fractionation between Li-bearing staurolite, Li-mica and aqueous fluids: An experimental study, *Chem. Geol.*, *238*(3–4), 277–290, doi:10.1016/j.chemgeo.2006.12.001.